

Detection of Thermoresponsive Polymer Phase Transition in Dilute Low-Volume Format by Microscale Thermophoretic Depletion

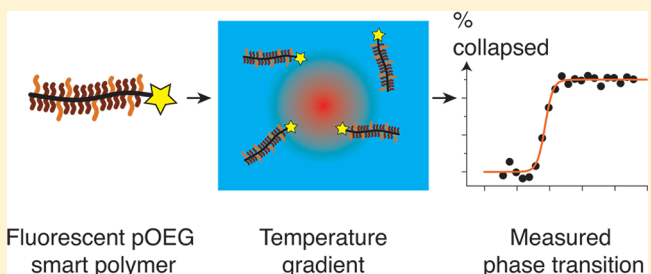
Manuel Wolff,^{†,‡} Dieter Braun,^{†,‡} and Michael A. Nash^{*,‡,§}

[†]Systems Biophysics, Ludwig-Maximilians-Universität, D-80799 Munich, Germany

[‡]Center for Nanoscience, Ludwig-Maximilians-Universität, D-80799 Munich, Germany

[§]Chair for Applied Physics, Biophysics and Molecular Materials, Ludwig-Maximilians-Universität, D-80799 Munich, Germany

ABSTRACT: Environmentally responsive polymers are becoming increasingly important in the biomaterials field for use as diagnostic reagents, drug carriers, and tissue engineering scaffolds. Characterizing polymer phase transitions by cloud point curves typically requires large milliliter volumes of sample at high micromolar solution concentrations. Here we present a method based on quantification of thermophoretic Soret diffusion that allows determination of polymer phase transitions using only $\sim 1 \mu\text{L}$ of liquid at dilute nanomolar concentrations, effectively reducing the amount of sample required by a factor of 10^6 . We prepared an oligo(ethylene glycol) (OEG) methyl ether methacrylate copolymer via RAFT polymerization. End-group modification with fluorescent BODIPY-maleimide provided a dye-labeled pOEG-BODIPY conjugate with a lower critical solution temperature (LCST) in the range of $\sim 25\text{--}35 \text{ }^\circ\text{C}$. Thermophoresis measurements in dilute solution demonstrated a marked change in polymer thermodiffusion in the vicinity of the LCST. We measured the temperature dependence of thermodiffusion and transformed these data sets into sigmoidal curves characterizing the phase transition of the polymer. Finite element modeling suggested a correction to the measured values that brought the transition temperatures measured by thermophoresis into accord with the cloud point curves. Our results demonstrate that observation of polymer thermodiffusion in a low volume dilute format is a facile method for determining polymer phase transition temperatures.



Fluorescent pOEG smart polymer Temperature gradient Measured phase transition

Environmentally responsive polymers represent a class of macromolecules with tunable properties that undergo dramatic conformational changes in response to slight changes in environmental conditions (e.g., temperature, pH, and light).^{1–6} Such polymers have been developed for use in biological applications, including as drug delivery vehicles,^{7,8} tissue engineering scaffolds,⁹ and reagents for affinity separation of diagnostic targets.¹⁰ Poly(*N*-isopropylacrylamide) (pNIPAm) is among the most widely studied thermoresponsive polymer systems, and attachment of this polymer to biological entities such as antibodies, enzymes, and nanoparticles has proven advantageous in biotechnology applications, including molecular diagnostics¹¹ and cell-surface interface engineering.¹² PNIPAm, however, also has associated limitations, including a significant hysteresis upon cooling. Due to intramolecular hydrogen bonding, it is generally difficult to completely rehydrate pNIPAm after hydrophobic collapse,¹³ requiring cooling well below the LCST.

More recently, polymers made from oligo(ethylene glycol) (OEG) have proven versatile both in terms of synthetic flexibility and biochemical properties.¹⁴ Poly-OEG (pOEG) consists of a hydrocarbon backbone with comblike OEG side chains of variable length. Poly(OEG) can be synthesized using a variety of living free radical polymerization methods, including ATRP and RAFT,^{15,16} facilitating control over molecular weight, block architecture, and functional end-

group incorporation. Although they are more hydrophobic than standard poly(ethylene glycol), pOEGs are still biocompatible and water-soluble. Moreover, pOEGs possess a temperature-responsive LCST behavior and have smaller hysteresis than pNIPAm. The transition temperature of pOEG can be tuned from $0\text{--}100 \text{ }^\circ\text{C}$, by varying the side-chain length of the OEG macromonomers.¹⁷

To measure the transition temperature of a polymer solution, light extinction is typically monitored as the temperature is slowly raised, resulting in a so-called “cloud point” curve describing the lower critical solution temperature (LCST). The cloud point process in fact involves two processes: the coil-to-globule transition of individual polymer chains and interchain aggregation that increases solution turbidity. Interactions with biomolecules can affect the LCST of biohybrid protein-polymer conjugates.¹⁸ This makes determining the precise transition point of a conjugate in specific biological milieu challenging. Performance of environmentally responsive materials *in vivo* may not be optimized correctly based on bulk cloud point measurements alone, therefore an assay to detect the transition point using small sample volumes at biologically relevant nanomolar solution concentrations would

Received: March 4, 2014

Accepted: May 12, 2014

Published: May 12, 2014

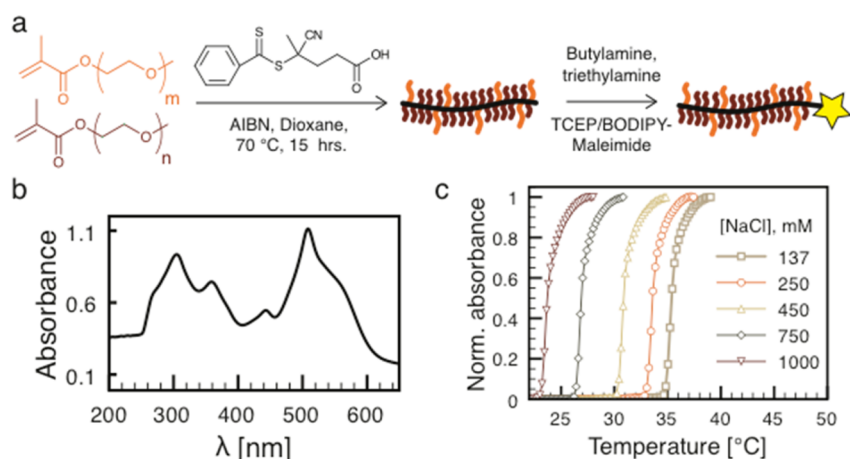


Figure 1. Preparation of an end-labeled thermoresponsive oligo(ethylene glycol) copolymer. (a) Copolymerization of oligo(ethylene glycol) methyl ether methacrylates ($n = 2$, $m = 8.5$) using a dithiobenzoate RAFT agent resulted in a thermoresponsive pOEG copolymer. Following purification and aminolysis of the RAFT agent, labeling of the resulting thiol groups with BODIPY-maleimide produced the final 100 kDa pOEG-BODIPY conjugate. (b) Absorbance spectrum of the polymer exhibited chromophore absorbance at 505 nm and peaks associated with the cleaved RAFT agent at 300 and 360 nm. (c) LCST behavior of the fluorescent copolymer in 10 mM phosphate buffered saline at pH 7.4 with variable NaCl showed a decrease in LCST with increasing NaCl. The LCST values were then compared with those determined from thermodiffusion measurements of the same samples.

be an advantage in conjugate optimization studies for biological applications.

Thermophoresis, or the Ludwig-Soret effect, describes the tendency of molecules to move along temperature gradients. Although the effect has been known for more than 150 years, the underlying theory is still fragmentary. Several predictions of the electrostatic and electrophoretic contributions to the Soret coefficient (S_T) have been supported by experimental data on DNA and charged beads,^{19–26} but the contribution of nonionic interactions remains less clear.^{27–29} Meanwhile, the importance of developing a solid theoretical framework is highlighted by several newly discovered applications of bioanalytics, bio-detection, and molecular trapping.^{30,31} Differences in thermal diffusion of a labeled binding partner can be used to detect the presence of a second binding partner. This assay format requires minimal sample volume and has proven facile, rapid, and compatible with a wide range of samples.³²

Hydration water and its associated entropy are also suspected to contribute to thermodiffusion. Since release of “caged” hydration water molecules is known to play a role in smart polymer phase transitions,³³ we postulated that a smart polymer system would be an informative sample for thermodiffusion measurements. We tested whether the thermodiffusion behavior of an environmentally responsive polymer would be indicative of its conformational changes near the LCST. A prior report on thermodiffusion of pNIPAm using a different measurement method (i.e., thermal diffusion forced Rayleigh scattering³⁴) also suggested the phase transition could potentially be observed in changes of the Soret coefficient with temperature. We selected a synthetic route that included cleavage of the RAFT chain transfer agent and subsequent modification with an uncharged BODIPY-FL derivative. This allowed the thermophoretic depletion to be measured using LED-induced fluorescence detection and IR-laser heating inside a microcapillary. The thermodiffusion of the thermoresponsive fluorescent polymer could therefore be directly characterized using small volumes and dilute solutions. A computational steady-state model was further used to validate the

experimental results and predict a correction to the experimental data.

RESULTS AND DISCUSSION

The synthetic steps en route to an end-labeled thermoresponsive pOEG polymer are shown in Figure 1a. The pOEG-BODIPY was synthesized using thermally initiated RAFT polymerization. We used a dithiobenzoate chain transfer agent together with AIBN as the thermally activated initiator. A RAFT agent to initiator ratio of 4:1 was used. The target molecular weight of the polymerization was 100 kDa. Poly(ethylene glycol)_{8.5} methyl ether methacrylate and di(ethylene glycol)₂ methyl ether methacrylate were loaded into the polymerization feed at a molar ratio of 1:4 (i.e., 20 mol % OEG_{8.5}). Our previous work had indicated that this ratio would provide an LCST of ~37 °C in standard PBS buffer containing 137 mM NaCl.¹⁵ Since OEG_{8.5} is more hydrophilic than OEG₂, inclusion of this monomer at higher loadings tended to decrease the transition temperature of resulting copolymers. Following purging with N₂ to remove inhibitory oxygen, the reaction proceeded for 15 h at 70 °C. The reaction mixture was then cooled and the product recovered by precipitation and dialysis. The molecular weight of the product was estimated by extinction spectrophotometry of the dithiobenzoate end group contained in the polymer prior to aminolysis (see Experimental Section). We determined the extinction coefficient of the chain transfer agent to be $\epsilon_{\lambda=300 \text{ nm}} = 1.47 \times 10^4 \text{ mol cm}^{-1}$, and the pOEG molecular weight to be $M_n = 92.3 \pm 6.5 \text{ kDa}$. Following purification, the polymer was freeze-dried and transferred into dimethylformamide for aminolysis. A 10-fold excess of triethylamine and butylamine was used to cleave the trithiocarbonate group at the end of the RAFT agent, resulting in a thiol group that could be modified directly with BODIPY FL-maleimide, as previously described.³⁵ Shown in Figure 1b is the absorbance spectrum of the polymer following BODIPY labeling. The absorbance spectrum exhibited peaks at 300, 360, and 510 nm with a chromophore shoulder extending out to 560 nm, consistent with successful aminolysis and fluorescent labeling of the polymer. Following fluorescent labeling, the

polymer was purified using aqueous HPLC, and a narrow sample fraction under the monomodal elution peak was collected to further decrease sample polydispersity prior to thermophoresis measurements. Figure 1c shows normalized cloud point curves of the BODIPY-labeled pOEG obtained in water with variable amounts of NaCl. An increase in the amount of NaCl clearly depressed the LCST values due to the well-known Hofmeister effect.³⁶

The experimental setup for measuring thermodiffusion is depicted in Figure 2a. An upright microscope was equipped

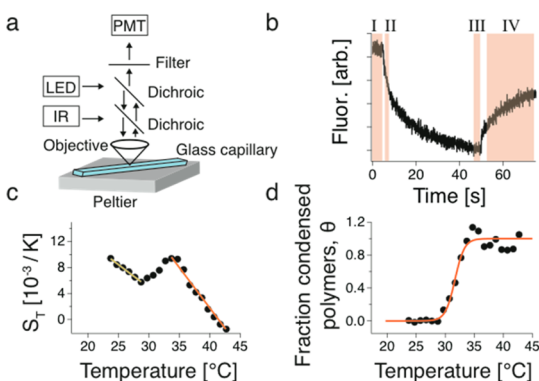


Figure 2. Measuring thermophoretic diffusion of thermoresponsive polymers. (a) Schematic of the setup. A photomultiplier tube (PMT) was inserted into the detection path of an epi-fluorescent microscope outfitted with a light emitting diode (LED) for fluorescence excitation, and an infrared (IR) laser for generating temperature gradients within the capillary. IR laser heating was used to induce Soret diffusion of the polymer sample. (b) Raw data trace showing a typical polymer thermodiffusion curve with regions as follows: region I, IR laser was off; region II, IR laser was on and fluorescence rapidly dropped due to temperature dependence of the dye; region III, near steady-state thermodiffusion of the sample occurred; region IV, IR laser was turned off and sample diffused back into the depletion zone. (c) The Soret coefficient (S_T) was calculated over a range of sample Peltier temperatures from time traces as in (b) using eq 1. (d) Thermal melting analysis (eq 3) was used to transform curves as in (c) into LCST curves that reported the transition temperature of the thermoresponsive polymer. The temperature axes show $T_0 + \Delta T/2$, as described in the finite element model (see below).

with a photomultiplier tube in the detection path, a cyan LED ($\lambda_{\text{ex}} = 505 \text{ nm}$) for fluorophore excitation, and an IR laser that locally heated the sample liquid within a confocal volume inside the rectangular glass microcapillary. Rectangular capillaries were used to minimize fluid transport due to thermal convection, which can confound thermodiffusion measurements.²⁰ The PMT was used to measure fluorescence emission from the same region of the sample that was heated by the IR laser, providing a measure of heat-induced depletion of fluorescently labeled polymer when the IR laser was switched on. Fluorescent labeling of the sample is therefore a prerequisite for the measurement. Thermophoresis curves in aqueous buffers were obtained following previously described protocols for such a setup.^{21,30,32,37} The fluorescence signal measured by the PMT was monitored over time within 4 distinct zones of the thermophoresis curve (Figure 2b). In zone I, the IR laser was off and the homogeneous fluorescence distribution within the capillary was nearly constant or decreasing slightly due to photobleaching. At $t = 5 \text{ s}$, the IR laser was switched on and a temperature gradient was quickly established on a short time scale ($\sim 50 \text{ ms}$). This temperature rise resulted in a rapid drop

in fluorescence (Figure 2b, II) due to an inherent temperature dependence of dye emission. Approximately 0.5 s of data following the switching on of the IR laser were excluded from the calculation of the intensity in zone II to exclude the temperature dependence of dye emission. After this temperature jump, the IR laser remained on while thermodiffusion took place on a slower timescale, eventually approaching a steady state at $t \approx 50 \text{ s}$ (Figure 2b, III). While the IR laser was on ($t = 5\text{--}50 \text{ s}$), the fluorescence intensity decreased monotonically, indicating that the labeled pOEG molecules were depleted from the heated zone and migrated toward the cooler zone, exhibiting a positive Soret coefficient. After a steady-state had been reached, the IR laser was switched off at time $t = 50 \text{ s}$, and the pOEG molecules diffused back into the now cool detection region for the remainder of the curve (Figure 2b, IV). The Soret coefficient, S_T , was calculated from such a curve, according to eq 1,

$$c_{\text{III}}/c_{\text{II}} = \exp(-S_T \Delta T) \approx 1 - S_T \Delta T \quad (1)$$

where $c_{\text{III}}/c_{\text{II}}$ is the average fluorescence in zone III divided by that of zone II and ΔT is the temperature difference between the hot and cold regions. Typically ΔT will depend on setup parameters such as IR laser power and capillary dimensions. We calibrated the setup using a pH/temperature sensitive dye 2',7'-bis (2-carboxyethyl)-5-(and-6) carboxyfluorescein (BCECF) and found that with rectangular capillary dimensions of $0.1 \times 1 \text{ mm}^2$, the temperature difference between hot and cold regions was $\Delta T = 9.4 \pm 0.8 \text{ K}$. Thermophoresis curves such as that shown in Figure 2b were collected over a range of Peltier base temperatures (T_0). From this data set, we were able to monitor how S_T changed with temperature as the polymer underwent its phase transition. On the basis of the results of a steady-state computational model described in further detail below, we corrected the temperature axis by adding $\Delta T/2$ to the Peltier base temperature (T_0). The temperature axes in Figures 2 and 3 therefore represent $T_0 + \Delta T/2$. Due to the temperature dependence of S_T , thermodiffusion of sample molecules is not constant but rather changes depending on a molecule's position within the Lorentzian temperature distribution imposed by IR heating, and this effect was accounted for with the correction of $\Delta T/2$. Apparently thermodiffusion in an inhomogeneous temperature field strictly averages to half of the peak thermal field as shown by simulations and calculations below.

As shown in Figure 2c, the Soret coefficient of pOEG in 450 mM NaCl exhibited three distinct zones with differing slopes. From 23–28 °C, a negative slope of $-7.1 \times 10^{-4} \text{ K}^{-1} \text{ }^\circ\text{C}^{-1}$ was obtained. In the intermediate range from 28–34 °C, a positive slope of $7.7 \times 10^{-4} \text{ K}^{-1} \text{ }^\circ\text{C}^{-1}$ was observed, while in the upper range again a negative slope of $-12.4 \times 10^{-4} \text{ K}^{-1} \text{ }^\circ\text{C}^{-1}$ was found. The two portions of the curve showing negative slope are fitted with solid lines. The absorbance cloud point curve (Figure 1c, 450 mM) for the same sample indicated the LCST of pOEG in 450 mM NaCl was $\sim 31 \text{ }^\circ\text{C}$. Since the S_T crossover point from negative to positive slope observed in Figure 2c occurred near the polymer LCST, we interpreted this zigzag pattern as an indication that the pOEG had two distinct thermodiffusion regimes above and below the cloud point. The positive slope portion of the curve near the LCST then represented the transition of pOEG from one regime to the other.

To assist in analysis and pinpoint the observed crossover point more precisely, we transformed the S_T versus temperature

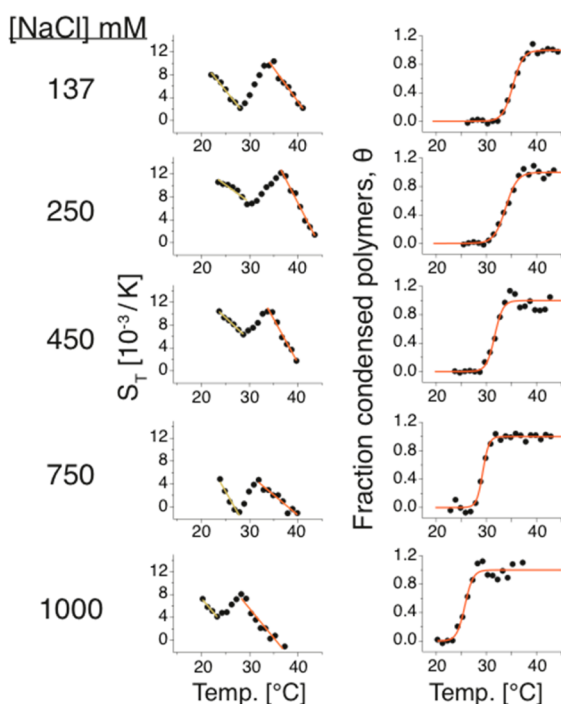


Figure 3. Characterization of Hofmeister effect on LCST using thermodiffusion measurements. Soret diffusion coefficients (S_T) and phase transition curves (θ) of the labeled pOEG copolymer at 1 nM (100 ng/mL) in PBS buffer with variable NaCl show that the transition temperature dropped steadily with increasing NaCl.

data into sigmoidal plots using an analysis method originally developed for thermal melting of DNA strands.³⁸ The results from such a transformation are shown in Figure 2d. We assumed the two thermodiffusion regimes fitted in Figure 2c with solid lines represented a two-state system. The fitted baseline from 23–28 °C we will call $S_{T,low}$. This equation of a line is a function of temperature and indicates the expected S_T values that would be measured if the whole system did not exhibit a phase transition. We call the fitted line from 35–43 °C, $S_{T,high}$, which indicates the expected S_T values for the system above the LCST, where the pOEG is collapsed and dehydrated. When the polymer underwent its transition, the S_T values we measured were in fact a superposition of S_T values from the fraction of molecules above transition (θ) together with the fraction of molecules below transition ($1 - \theta$). Since $S_{T,low}$ and $S_{T,high}$ are linear with respect to temperature, the measured signal can be expressed according to eq 2:

$$S_{T,measured} = \theta S_{T,high} + (1 - \theta) S_{T,low} \quad (2)$$

Rearranging and solving for θ , we obtained the following expression for the fraction of condensed polymers, eq 3:

$$\theta = \frac{S_{T,measured} - S_{T,low}}{S_{T,high} - S_{T,low}} \quad (3)$$

We note that $S_{T,low}$ and $S_{T,high}$ are both linear functions of temperature and are evaluated at the temperature at which $S_{T,measured}$ was determined. From these transformed data, we could then obtain a sigmoid fit using the Hill equation (Figure 2d, solid line) and determine the midpoint of the transition. The midpoint of the phase transition in this case was found to be 31.6 ± 0.15 °C, in agreement with the $Abs_{50\%}$ cloud point measurement of 30.9 ± 0.3 °C. It is important to note here that

correction of the base temperature T_0 by adding $\Delta T/2$ was required to achieve agreement between the cloud point and thermophoresis data. This correction was supported by the finite element model described below.

The key finding here is that differences in thermodiffusion behavior of the polymer molecules are indicative of its conformational change. The S_T curves were obtained in dilute solution (~ 1 nM or 100 ng/mL) on a timescale of 50 s. Since the polymer design ensured an uncharged molecule save only a single ionizable carboxyl group at the polymer's ω end, ionic contributions to Soret diffusion are kept to a minimum. The ionic contribution to Soret diffusion might otherwise overwhelm the signal and no transition behavior would be observed in S_T .

To further confirm that the changes in S_T that we measured were in fact indicative of the phase transition, we obtained thermophoresis curves for pOEG over a range of base temperatures (T_0) and salt concentrations from 137–1000 mM NaCl. We performed data analysis as described above by first fitting linear regions of the S_T versus temperature curve, and then transforming the data into a format that could be fitted with a sigmoidal function to estimate the transition temperature under each buffer condition. The results from such an experiment are shown in Figure 3. The midpoints of the fitted sigmoidal curves (Figure 3, right column) steadily shifted to lower temperatures as the amount of NaCl increased, consistent with the Hofmeister effect that was observed in the absorbance cloud point curves.

A comparison between the absorbance-based cloud points and the thermophoresis-based transition temperatures is presented in Table 1. On the basis of this comparison, it is

Table 1. Comparison of pOEG Transition Temperatures Determined Using Thermophoresis and Absorbance-Based Cloud Point Curves^a

[NaCl] (mM)	θ midpoint (°C)	Abs. cloud point (°C)
137	35.3 ± 0.34	35.4 ± 0.3
250	33.8 ± 1.89	33.6 ± 0.3
450	31.6 ± 0.15	30.9 ± 0.3
750	29.3 ± 0.46	26.9 ± 0.3
1000	25.7 ± 1.34	25.7 ± 0.3

^aThe errors for θ indicate \pm one standard deviation of the midpoint fit parameter of the Hill equation. The absorbance cloud point was defined as the temperature that reached 50% maximal absorbance. The 0.3 °C error for all cloud points represents the resolution of the temperature controller used in the extinction spectrophotometer.

clear that the thermophoresis result is consistent with the cloud point method and reproduces the transition points with high accuracy. The thermophoresis measurement, however, had several advantages, such as requiring 1000-fold less sample (~ 1 μ L instead of 1 mL). Additionally more dilute samples could be used because the fluorescence measurement was much more sensitive than the absorbance-based measurement. Cloud point curves are typically obtained using a high concentration of the polymer (e.g., \sim micromolar or milligram per milliliter range) in order to produce a sharp rise in signal at the characteristic temperature. Our thermophoresis-based measurement allowed us to measure the transition temperature using concentrations of only ~ 1 nM (100 ng/mL). This concentration range could be an advantage when studying interactions between thermoresponsive polymers and biological compo-

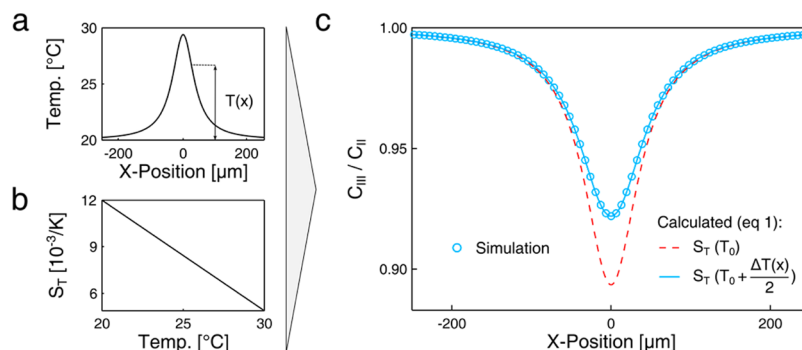


Figure 4. Finite element model of the system predicts a base temperature correction of $\Delta T/2$. (a) A Lorentzian temperature distribution was centered at the origin with a height of $T_0 + \Delta T = 20 + 9.4$ °C. (b) The temperature dependence of the Soret coefficient S_T was assumed linear over the range from 20–30 °C. (c) Simulation result (○) showing fluorescence depletion (C_{III}/C_{II}) calculated from a steady-state finite element model of transport eq 4. The C_{III}/C_{II} fluorescence depletion predicted by eq 1, assuming an S_T equal to $12 \times 10^{-3} \text{ K}^{-1}$ [i.e., S_T at the base temp, $S_T(T_0)$] overestimates thermophoretic depletion (red dashed line). Correcting S_T by an amount corresponding to $S_T(T_0 + \Delta T(x)/2)$ results in good agreement between eq 1 and the finite element simulation (blue solid line).

nents, which may themselves be present only in exceedingly low quantities (e.g., < nanomolar).

To understand the interplay between the base temperature and the observed thermodiffusion coefficients (S_T), we used a finite element method to model the system at steady state. An overview of the modeling results is shown in Figure 4. Two sets of given information went into the simulation. First, the temperature distribution was assumed to Lorentzian (Figure 4a) with base temperature $T_0 = 20$ °C, a ΔT at the peak of 9.4 °C, and a laser spot size of 40 μm according to the relation $T = 20 \text{ °C} + 9.4 \text{ °C} [1/(1 + (x/40 \mu\text{m})^2)]$. Second, the temperature dependence of the Soret coefficient (Figure 4b) was considered to be linear with temperature and follow the relation: $S_T(T) = 2.6 \times 10^{-2} \text{ K}^{-1} - 7.1 \times 10^{-4} \text{ K}^{-1} \text{ °C}^{-1} \times T$. We furthermore presumed a concentration of 1 at the boundaries. At steady state, we assumed the net flux of molecules at each position was zero according to eq 4,

$$j_D = -D\nabla C - S_T DC \nabla T = 0 \quad (4)$$

where j_D is the molecular flux, D is the diffusion coefficient, C is the polymer concentration, S_T is the Soret coefficient, and T is the temperature. This transport equation accounts for diffusion of the sample in the first term and thermodiffusion in the second term. At steady state, $j_D = 0$ and the diffusive flux is equal to the negative of the thermodiffusive flux. Since D appears in both fluxes, it cancels out for the steady state and the solution is independent of the diffusion coefficient. This steady state equation along with the two given sets of information were programmed into a finite element modeling program (FEM-LAB), and the normalized 1D concentration was determined at each point. The size of the bounding simulation box was kept very large (50000 μm) to minimize edge effects. The results from such a simulation are shown in Figure 4c (right plot, blue ○). The simulation result confirmed that thermophoretic depletion of pOEG from the heated zone should occur in accordance with the positive Soret coefficients across this temperature range. It also estimated the magnitude of this depletion given the Lorentzian temperature profile, and the temperature-dependence of the thermodiffusion behavior.

In a second step, we calculated the expected C_{III}/C_{II} distribution based on eq 1. We determined how well eq 1 predicted the simulated C_{III}/C_{II} profile given a correction to the Soret coefficient. We calculated C_{III}/C_{II} at every point from eq 1 by plugging in a S_T at the base temperature $T_0 = 20$ °C and a

$\Delta T(x) = T(x) - T_0$ or the distance-dependent temperature difference from the base temperature. We found that with no correction, eq 1 overestimated the depletion in comparison with the finite element model (Figure 4, right plot, dotted red line). When we corrected the S_T values by assuming $S_T = S_T(T_0 + \Delta T(x)/2)$, eq 1 was found to be consistent with the steady-state simulation (Figure 4, right plots, solid blue line). This accordance between the steady-state solution and eq 1 with a corrected S_T value supported the interpretation that the finite steepness of the temperature gradient necessitated a correction to the measured S_T values or rather a shift in the temperature axis from T_0 to $T_0 + \Delta T/2$. Apparently molecules with Soret coefficients that are linearly dependent on temperature establish a concentration profile in a Lorentzian temperature field according to Soret coefficients evaluated at a temperature of $T_0 + \Delta T(x)/2$, following eq 5,

$$\ln[c(x)/c_0] = -S_T|_{T_0+\Delta T(x)/2} \cdot \Delta T(x) \quad (5)$$

This correction holds for all kinds of microscale thermophoresis measurements and implies that the finite steepness of the temperature profile should, for example, also be taken into account in analysis of temperature-dependent binding curves or thermophoresis experiments on protein unfolding. However, it remains to be determined if the $\Delta T/2$ correction also holds for systems with a nonlinear temperature dependence of S_T or for non-Lorentzian temperature distributions.

Since the C_{III}/C_{II} fluorescence ratios that were measured experimentally were analyzed using eq 1 to obtain relevant Soret coefficients, the simulation results imply a temperature axis shift by $\Delta T/2$ is required. It is noted that the correction in this case was necessary to bring the transition temperatures determined by thermodiffusion into agreement with the LCST cloud points. This is also a further confirmation of the validity of the model, since the transition point of the polymer is expected to be independent of the method used to measure it.

In summary, we prepared a thermoresponsive pOEG polymer using RAFT polymerization and fluorescently tagged the polymer with an uncharged fluorophore using aminolysis in tandem with maleimide-BODIPY labeling. We characterized the LCST of the fluorescently labeled pOEG as a function of added NaCl using cloud point curves and further investigated pOEG thermodiffusion behavior over base temperatures (T_0) that ranged above and below the LCST. A correction to the temperature axis from T_0 to $T_0 + \Delta T/2$ that was predicted by a

finite element steady-state model brought the LCST values determined by thermodiffusion measurement into accord with those determined using conventional cloud point curves. By transforming the data using an analysis method originally developed for DNA melting curves, we found that the phase transition could be accurately determined based solely on thermodiffusion data. The measurement was performed at a polymer concentration of ~ 1 nM (100 ng/mL) using only ~ 1 μ L of sample, making our approach compatible with determination of polymer LCST at low concentrations in biological milieu (e.g., small volume cell lysate). Since both thermophoresis and thermoresponsive polymers are compatible with measurement in biological liquids,^{32,39} moving into biological liquids should be straightforward with this method and requires further experimental work. This approach should prove useful for determining phase transition behavior of biohybrid environmentally responsive polymer systems in a low-volume dilute format.

■ EXPERIMENTAL SECTION

Polymer Synthesis. Oligo(ethylene glycol)_{8.5} methacrylate (M_n 475, 100 ppm MEHQ, 200 ppm BHT inhibitor, product number 447943) and di(ethylene glycol)₂ methyl ether methacrylate (M_n 188.22, 95% pure, product number 447927) were purchased from Sigma and purified through a neutral aluminum oxide column prior to use. The RAFT chain transfer agent 4-cyano-4-(phenylcarbonothioylthio)pentanoic acid (DTB, M_n 279.38, 97% pure, product number 722995) was purchased from Sigma and used as received. The initiator 2,2'-azobis(2-methylpropanitrile) (AIBN, M_n = 164.21) was purchased from Sigma and recrystallized from methanol. In a typical polymerization with a target molecular weight of 100 kDa, a reaction vial with Teflon stopper was loaded with 1.6 g of di(ethylene glycol) methyl ether methacrylate and 0.4 g of the oligo(ethylene glycol)_{8.5} methacrylate. Next, 6.4 mg of the DTB chain transfer agent and 540 μ g of the initiator dissolved in dioxane were added. Two grams of dioxane were then added such that the mass ratio of dioxane to monomers was 1:1. The flask was purged for 30 min with N₂. The reaction proceeded at 70 °C for 17 h and was then precipitated into hexane at 4 °C. The precipitate was next dissolved into tetrahydrofuran and precipitated two more times into chilled hexane. Finally, the product was collected by centrifugation, dried under vacuum, and recovered via dialysis and lyophilization.

Aminolysis and BODIPY Labeling. The lyophilized polymer was dissolved at 300 mg/mL in dimethylformamide (DMF). A 10-fold excess of butyl amine and triethylamine were added, and the reaction proceeded overnight at room temperature. The reaction progress was monitored by UV-spectrophotometry. The product was recovered via precipitation into an ice cold 1:1 hexane:ether mixture, followed by drying under vacuum. Next the polymer was dissolved in PBS buffer, pH 7, 4 °C, 2 mg/mL. Ten microliters TCEP disulfide reducing slurry (Pierce) per milliliter polymer solution was added. The TCEP slurry was mixed with polymer for 1–2 h at room temperature and removed via centrifugation. The BODIPY-maleimide dye was dissolved at 10 mM in DMF and added in a 10-fold molar excess to the polymer in PBS buffer. The reaction was allowed to proceed overnight at 4 °C. The product was recovered using gel filtration (GE Healthcare PD-10 column) and HPLC.

Polymer Analysis. To estimate the molecular weight of the polymer, the molar extinction coefficient of the DTB chain

transfer agent was determined. Since DTB is not water-soluble, we first determined the molar extinction coefficient of DTB in methanol (see main text). Next, the polymer absorbance at known mass concentrations was determined in both water and methanol. The DTB molar extinction coefficient was then corrected by the ratio of polymer absorbance in water/methanol. This provided a measure of the molarity of DTB and therefore polymer chains in the aqueous polymer sample. On the basis of this mass/molarity ratio, we calculated the average molecular weight of the polymer to be $M_n = 92.3 \pm 6.5$ kDa. To further decrease polydispersity prior to thermophoresis measurements, HPLC (GE Äkta, Superdex gel filtration media) was used to isolate a narrow fraction under the primary monomodal elution peak.

Absorption Spectrophotometry. Cloud point curves of the polymer dissolved at 1 mg/mL in water with variable NaCl were obtained using a UV-vis spectrometer (Jasco GmbH, Germany) equipped with a temperature controller (PAC-743) with control accuracy of ± 0.3 °C. We acquired an absorbance spectrum of our sample at 15 °C and blanked the instrument. Next a heating ramp of 0.3 °C/min was applied, with measurements taken every 0.2 °C at a wavelength of 400 nm. We used a sample volume of 1 mL in poly(styrene) cuvettes with an optical path length of 1 cm. Data curves were normalized by the maximal absorbance above transition.

Thermophoresis Measurements. The thermophoresis measurement setup has been described previously.^{20,31,32} We modified an AxioScope Vario fluorescence microscope (Carl Zeiss GmbH, Germany) with a 1480 nm IR laser (Fibotec Fiberoptics, Germany). A Partec Objective (40 \times , 0.80 mm working distance, 0.8 NA) was used to focus both LED excitation light and IR laser light. The pOEG polymer was dissolved at 1 nM (100 ng/mL) in phosphate-buffered saline/Roti-block (nonspecific blocker, Carl Roth) with variable amounts of NaCl. Polymer samples were loaded into rectangular borosilicate capillaries with dimensions of 0.1 \times 1 mm² (Vitrocom, Mountain Lakes, NJ) by capillary action within a few seconds. Afterward, the open ends were sealed with wax (Tight Sealing Wax, NanoTemper, Munich, Germany) and the outer surface cleaned with isopropyl-alcohol and a piece of clean tissue. Then the capillaries were placed on a Peltier element and heated from below. The base temperature T_0 of the Peltier element was set using feedback control programmed in LabView. The C_{III}/C_{II} fluorescence ratios were determined by averaging the PMT signal over a time period of 2 s within the respective regions of the thermophoresis curves.

■ AUTHOR INFORMATION

Corresponding Author

*E-mail: michael.nash@lmu.de.

Notes

The authors declare no competing financial interest.

■ ACKNOWLEDGMENTS

The authors gratefully acknowledge a joint grant to D.B. and M.A.N. from the LMU Center for Nanoscience (CeNS). Financial support from the NanoSystems Initiative Munich and European Research Council Starting Grant is acknowledged. M.A.N. acknowledges funding from the Alexander von Humboldt Foundation and from Society in Science – The Branco Weiss Fellowship administered by the Swiss Federal Institute of Technology (ETH) Zürich, Switzerland. The

author's thank Christof Mast, Mario Herzog, Maren Reichl, Thomas Nicolaus, and Benjamin Böhm for helpful discussions and assistance with thermophoresis measurements.

REFERENCES

- (1) Hoffman, A. S.; Stayton, P. S. *Prog. Polym. Sci.* **2007**, *32*, 922–932.
- (2) Kumar, A.; Srivastava, A.; Galaev, I. Y.; Mattiasson, B. *Prog. Polym. Sci.* **2007**, *32*, 1205–1237.
- (3) Nash, M. A.; Lai, J. J.; Hoffman, A. S.; Yager, P.; Stayton, P. S. *Nano Lett.* **2010**, *10*, 85–91.
- (4) Smith, A. E.; Xu, X.; McCormick, C. L. *Prog. Polym. Sci.* **2010**, *35*, 45.
- (5) Gil, E. S.; Hudson, S. M. *Prog. Polym. Sci.* **2004**, *29*, 1173–1222.
- (6) Stuart, M. A. C.; Huck, W. T. S.; Genzer, J.; Müller, M.; Ober, C.; Stamm, M.; Sukhorukov, G. B.; Szleifer, I.; Tsukruk, V. V.; Urban, M.; Winnik, F.; Zauscher, S.; Luzinov, I.; Minko, S. *Nat. Mater.* **2010**, *9*, 101–113.
- (7) Qiu, Y.; Park, K. *Adv. Drug Delivery Rev.* **2012**, *64*, 49–60.
- (8) Schmaljohann, D. *Adv. Drug Delivery Rev.* **2006**, *58*, 1655–1670.
- (9) Furth, M. E.; Atala, A.; Van Dyke, M. E. *Biomaterials* **2007**, *28*, 5068–5073.
- (10) Nash, M. A.; Waitumbi, J. N.; Hoffman, A. S.; Yager, P.; Stayton, P. S. *ACS Nano* **2012**, *6*, 6776–6785.
- (11) Nash, M. A.; Yager, P.; Hoffman, A. S.; Stayton, P. S. *Bioconjugate Chem.* **2010**, *21*, 2197–2204.
- (12) Yang, J.; Yamato, M.; Shimizu, T.; Sekine, H.; Ohashi, K.; Kanzaki, M.; Ohki, T.; Nishida, K.; Okano, T. *Biomaterials* **2007**, *28*, 5033–5043.
- (13) Lutz, J.-F.; Akdemir, Ö.; Hoth, A. *J. Am. Chem. Soc.* **2006**, *128*, 13046–13047.
- (14) Gao, W.; Liu, W.; Christensen, T.; Zalutsky, M. R.; Chilkoti, A. *Proc. Natl. Acad. Sci. U.S.A.* **2010**, *107*, 16432–16437.
- (15) Nash, M. A.; Gaub, H. E. *ACS Nano* **2012**, *6*, 10735–10742.
- (16) Lutz, J.-F. *J. Polym. Sci. A, Polym. Chem.* **2008**, *46*, 3459–3470.
- (17) Lutz, J.-F. *Adv. Mater.* **2011**, *23*, 2237–2243.
- (18) Buller, J.; Laschewsky, A.; Lutz, J.-F.; Wischerhoff, E. *Polym. Chem.* **2011**, *2*, 1486.
- (19) Reineck, P.; Wienken, C. J.; Braun, D. *Electrophoresis* **2010**, *31*, 279–286.
- (20) Jerabek-Willemsen, M.; Wienken, C. J.; Braun, D.; Baaske, P.; Duhr, S. *ASSAY and Drug Development Technologies* **2011**, *9*, 342–353.
- (21) Wienken, C. J.; Baaske, P.; Duhr, S.; Braun, D. *Nucleic Acids Res.* **2011**, *39*, e52–e52.
- (22) Mast, C. B.; Braun, D. *Phys. Rev. Lett.* **2010**, *104*, 10410.1103/PhysRevLett.104.188102.
- (23) Schoen, I.; Krammer, H.; Braun, D. *Proc. Natl. Acad. Sci. U.S.A.* **2009**, *106*, 21649–21654.
- (24) Duhr, S.; Braun, D. *Proc. Natl. Acad. Sci. U.S.A.* **2006**, *103*, 19678–19682.
- (25) Putnam, S. A.; Cahill, D. G. *Langmuir* **2005**, *21*, 5317–5323.
- (26) Dhont, J. K. G.; Wiegand, S.; Duhr, S.; Braun, D. *Langmuir* **2007**, *23*, 1674–1683.
- (27) Stadelmaier, D.; Köhler, W. *Macromolecules* **2008**, *41*, 6205–6209.
- (28) Würger, A. *Phys. Rev. Lett.* **2009**, *102*, 078302.
- (29) Kita, R.; Wiegand, S.; Luettmer-Strathmann, J. *J. Chem. Phys.* **2004**, *121*, 3874.
- (30) Wienken, C. J.; Baaske, P.; Rothbauer, U.; Braun, D.; Duhr, S. *Nat. Commun.* **2010**, *1*, 100.
- (31) Lippok, S.; Seidel, S. A. I.; Duhr, S.; Uhland, K.; Holthoff, H.-P.; Jenne, D.; Braun, D. *Anal. Chem.* **2012**, *84*, 3523–3530.
- (32) Seidel, S. A. I.; Dijkman, P. M.; Lea, W. A.; van den Bogaart, G.; Jerabek-Willemsen, M.; Lazic, A.; Joseph, J. S.; Srinivasan, P.; Baaske, P.; Simeonov, A.; Katritch, I.; Melo, F. A.; Ladbury, J. E.; Schreiber, G.; Watts, A.; Braun, D.; Duhr, S. *Methods* **2013**, *59*, 301–315.
- (33) Deshmukh, S. A.; Sankaranarayanan, S. K. R. S.; Suthar, K.; Mancini, D. C. *J. Phys. Chem. B* **2012**, *116*, 2651–2663.
- (34) Kita, R.; Wiegand, S. *Macromolecules* **2005**, *38*, 4554–4556.
- (35) Scales, C. W.; Convertine, A. J.; McCormick, C. L. *Biomacromolecules* **2006**, *7*, 1389–1392.
- (36) Cho, Y.; Zhang, Y.; Christensen, T.; Sagle, L. B.; Chilkoti, A.; Cremer, P. S. *J. Phys. Chem. B* **2008**, *112*, 13765–13771.
- (37) Baaske, P.; Wienken, C. J.; Reineck, P.; Duhr, S.; Braun, D. *Angew. Chem., Int. Ed.* **2010**, *49*, 2238–2241.
- (38) Mergny, J.-L.; Lacroix, L. *Oligonucleotides* **2003**, *13*, 515–537.
- (39) Stocker, G.; Vandevyver, C.; Hilbrig, F.; Freitag, R. *Biotechnol. Prog.* **2006**, *22*, 1621–1629.